A Hologram Reconstruction Algorithm for Landmine Recognition and Classification Based on Microwave Holographic Radar Data

G. Borgioli[1], L. Bossi[1], L. Capineri[1], P. Falorni[1], T. Bechtel[2], F. Crawford[2], M. Inagaki[4], G. Pochanin[3], V. Ruban[3], L. Varyanitza-Roschupkina[3], and T. Ogurtsova[3]

[1]University of Florence, DINFO, Italy
[2]Franklin and Marshall College, PA, USA
[3]Usikov Institute for Radiophysics and Electronics
National Academy of Sciences of Ukraine, Ukraine
[4]Walnut Ltd., Japan

Abstract— We have developed a stand-off holographic subsurface radar (HSR) operating at 2 GHz with amplitude and phase outputs for detection and classification of buried shallow objects, including plastic landmines. The microwave holograms obtained in this way contain information about the size and shape of the buried objects within the penetration depth. The reconstruction of the electromagnetic field on a plane parallel to the scanning plane has been repeatedly addressed in the literature; however, the propagation of the incident field through the air-soil interface generates a refracted path into air and soil with a different velocity and thus results in different phase changes. Furthermore, the actual dimensions of the antenna aperture in relation to the scanning surface and the real radiation pattern are to be considered. In this work, we define and test an algorithm that uses the amplitude and phase data derived from the use of a finite-sized monostatic antenna. The antenna, with an aperture comparable to the buried object size (circular aperture of 11.5 cm of diameter), is positioned at few centimetres from the ground, and scans an area containing the buried object to provide the basic hologram. We have investigated the proposed method to assess the improvement in the detection of buried objects.

1. INTRODUCTION

A stand-off holographic subsurface radar (HSR) is realized, having a circular waveguide antenna with two feeds, one for transmitting a signal (a continuous wave at a frequency of 2 GHz), and one for receiving a signal. The hologram is formed by the interference between the direct coupling and the received signal from the antenna. Figure 1 shows a block diagram of this radar system.

In this system, the voltage controlled oscillator (VCO) generates the signal $v_t(t)$ for the antenna transmitting feed (TX). The same signal is sent to a phase/amplitude comparator (AD8302), which provides the two voltages: V_{MAG} and V_{PHS}. V_{MAG} is proportional to the log-ratio of the voltages of the two input signals, and V_{PHS} is proportional to the difference between the phases of the two signals. According to the holographic imaging principle, the receiving feed (RX) registers both the direct coupling signal from the transmitting feed and the signal reflected by the target lying in a plane at a distance z_0. This signal $v_{ar}(t, z_0)$ is compared to the signal $v_t(t)$ by the comparator AD8302.

The usefulness of such an instrument for the detection of buried objects has been previously demonstrated, but its full capability for this task can truly be obtained when it is mounted on a mechanical scanner that operates at a certain distance from the soil surface [1, 2]. In our system, the HSR is mounted on a fast mechanical scanner capable of operating outdoors with uniform spatial sampling of 5 mm by 5 mm over an area as large as 300 mm × 300 mm. The digitally-recorded microwave holograms contain detailed information about the size and shape of buried objects within the effective signal penetration depth. In our case we assume a 20-cm penetration depth in an average soil with relative permittivity ε_{rel} between 2 and 4. However, the propagation of the incident field through the air-soil interface generates a refracted path into air and soil with a different propagation velocity, resulting in different phase changes. These problems concerning the application of holographic imaging in the field have been identified in previous work [3, 4], but robust solutions to these problems have not yet been found.

In this work, we propose and test an algorithm that uses the holographic amplitude and phase data from a regularly-sampled grid to generate high-resolution plan-view images of buried objects. The algorithm remains under study and is subject to modification as this work proceeds.

The theoretical resolution of a holographic radar used in contact with the irradiated medium, is around a quarter of the wavelength of the signal. For a working frequency of 2 GHz, this corresponds

to an in-plane resolution of about 3.75 cm. The need to irradiate in air, at a known distance from the medium in which the object is buried, inevitably degrades the theoretical limit. The goal of this algorithm is to reach this limit and thereby identify the essential details of the target (shape and dimensions) in order to differentiate between different types of objects. For this reason, a standard compact disk (CD) was chosen as test object because of its simple shape (a planar reflector) with a central hole with size comparable with the theoretical resolution limit of the radar. In the algorithm development, we assumed that the propagation medium was homogeneous and non-dispersive.

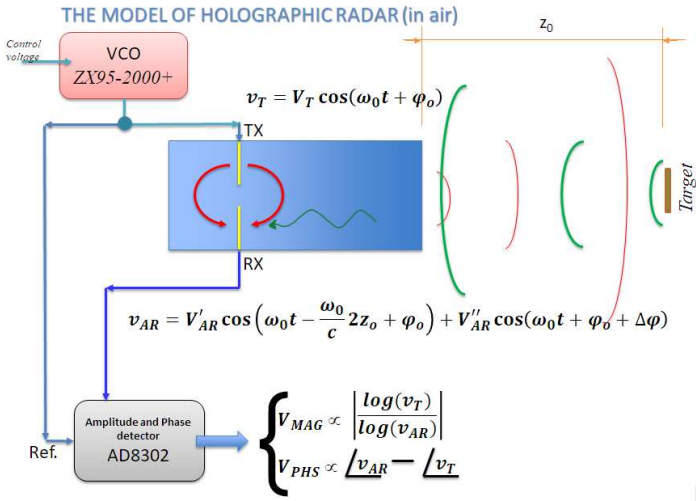

Figure 1: Block scheme of the 2 GHz holographic radar.

2. METHOD

The method is a revised implementation of the theoretical formulation described in [5] and comprehends the finite dimensions of the antenna aperture and the actual beam shape. Figure 2 illustrates the reference coordinate system [6]; the left side shows the circular aperture of the antenna on the scanning plane with a diameter $D = 2a = 115$ cm (where a is the radius); the right side shows the plane in which the target lies.

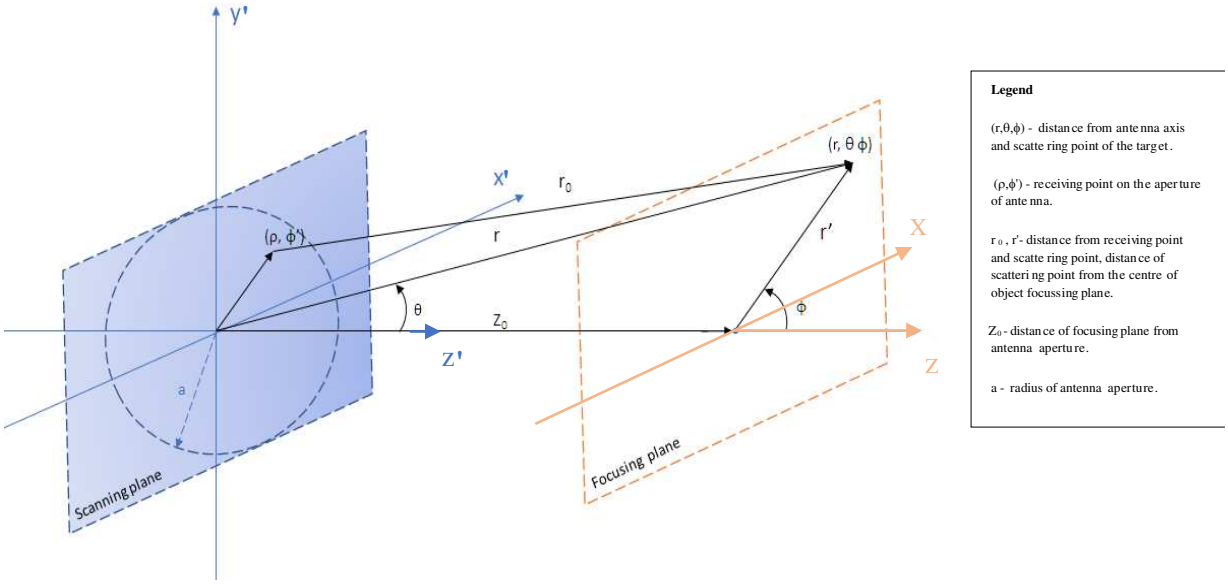

Figure 2: Coordinate systems of the model.

Figure 3 shows the block diagram of the proposed algorithm as developed in MATLAB. We note that these steps can be executed quickly enough to be used in quasi real-time at the end of

the mechanical acquisition.

The complete algorithm consists of five steps as described below:

1. Data acquisition from antenna system takes place by sampling a 31 cm × 17 cm scanning area at a step of 5 mm in both dimensions. The output of the block is a matrix of magnitudes and phases. The size of the scanning area is wide enough to acquire complex voltage values (V_{MAG}, V_{PHS}) generated by the main propagation lobe of the buried objects that were considered in our experiments (see Figure 8(a)). The two analog signals V_{MAG} and V_{PHS} are sampled with 16 bit analog-to-digital converters (ADC) with an input dynamic range of 3.6 V.
2. The output of the antenna system represents the interference between the direct coupling signal and reflection from any buried targets. Thus, it is normalised to estimate the electromagnetic field integrated over the antenna aperture.
3. The third block removes the effects of a non-point-like antenna aperture. The aperture sensitivity function is deconvolved from the normalised signal to account for the effect of the non-uniform radiation pattern over the finite size of antenna aperture (Figure 8(c)). In fact, the function $s(x', y')$ reported in [7] refers to the value of the electromagnetic field at a point while in a real experiment the value is averaged over the entire antenna aperture. The point spread function $PSF_1 = (1-(\frac{\rho}{a})^2)^n$ is the one used in [8] to describe the electromagnetic field distribution over the aperture, where ρ is the radial distance from antenna aperture centre, n is an exponent that depends on the employed antenna and a is the antenna aperture radius. The deconvolution is performed with the MATLAB function "*deconvlucy*" with the parameter $n = 2$. The output of this block is the representation of the electric field $E(x', y')$ on the scanning plane without the averaging effect introduced by the extended surface of antenna aperture.
4. According to [5], the reconstruction of the electromagnetic field at distance z_0 from the antenna aperture is $(\hat{I}(x, y, z_0))$ (Figure 3). The method is an approximation because it neglects both the radiation pattern and attenuation with distance. However, the results are still usable if it is sufficient to simply define the general target shape. An example of this block output (where the object is focused at $z_0 = 3$ cm) is shown in Figure 8(d).
5. Defocussing takes place due to the divergence of the transmitted beam. To overcome this effect, another deconvolution is performed on the focussed signal by generating another point spread function; PSF_2 (Figure 5) estimated by a blind deconvolution method using the MATLAB function *"deconvblind"*. The function uses the maximum likelihood algorithm and an initial guess (a matrix of ones) of the point spread function.

The actual deconvolution is applied with the *deconvlucy* MATLAB function using the estimated point spread function (see Figure 8(e)).

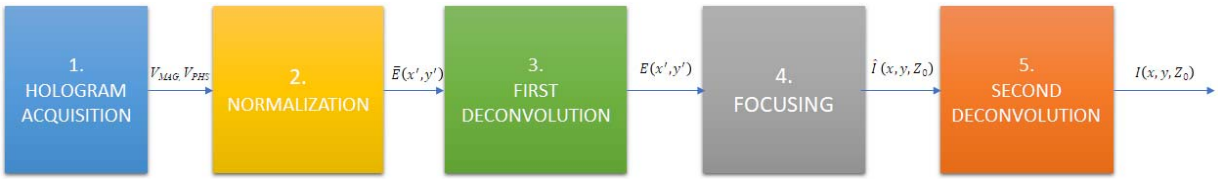

Figure 3: Block scheme of hologram deconvolution process.

3. EXPERIMENTS

Experiments were carried-out by mounting the HSR antenna on a three-axis movement system that can cover a scanning area of 31 cm × 16.5 cm (see Figure 6). The present system configuration does not allow a lateral scan larger than 16.5 cm, which just suitable to pick up the main interference lobe of the diffraction pattern. The next version of the scanner will have a wider lateral range to manage larger objects.

In the experiments, the antenna radiates while it moves over sand in a wooden box. The sand layer thickness is 20 cm from the bottom floor of the box, and the sand surface has been manually smoothed. For the targets, two types of reflectors were chosen: a standard Compact Disk and a PMN-4 type anti-personnel mine simulant. The compact disk is used as a clutter object that is

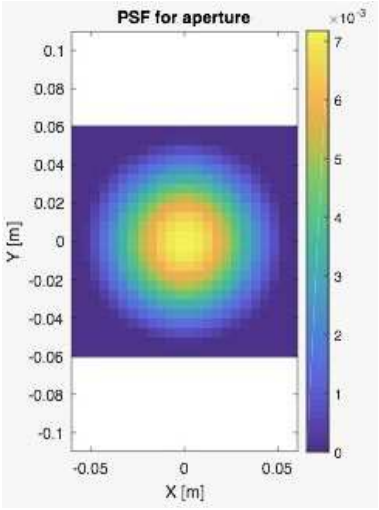

Figure 4: PSF_1 (Point Spread Function) for the deconvolution of the extended antenna aperture effect.

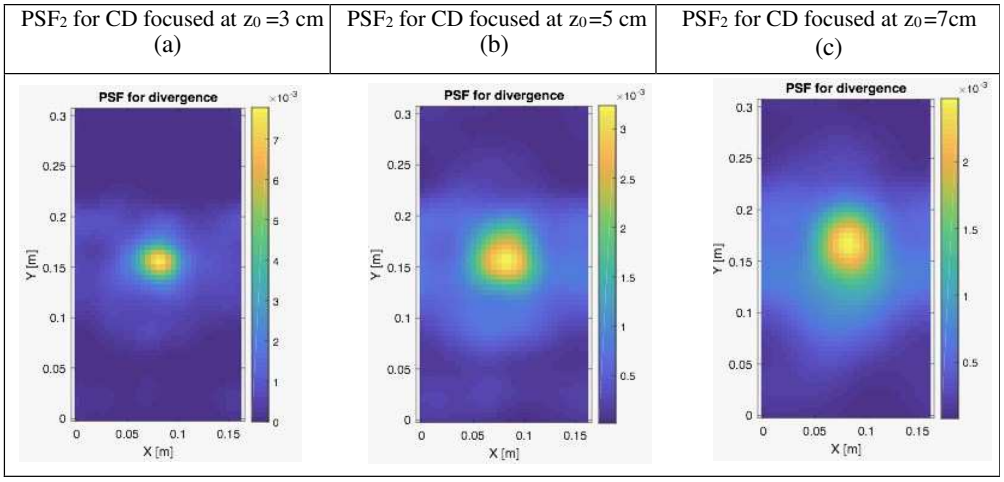

Figure 5: Calculated point spread function PSF_2 for the compact disk target focused at different distances (z_0) from the scanning plane.

Figure 6: Pictures of the scanned area and the experimental setup with a CD in shallow sand.

well-characterized electromagnetically as a planar reflector. The size and approximate shape of the two targets are shown in Figure 7.

Figure 8 shows the output amplitude from each step in the processing chain (blocks a, b, c, d, and e).

We can see in Figure 8 that after acquisition (Figure 8(a)), the amplitude has a dynamic range of about 2.5 mV, or from 22.5 mV to 25 mV. The circular shape of the CD is laterally distorted, probably due to the presence of reflections from the vertical sides of the sandbox.

After normalization (Figure 8(b)), the dynamic range remains unchanged, but the levels drop

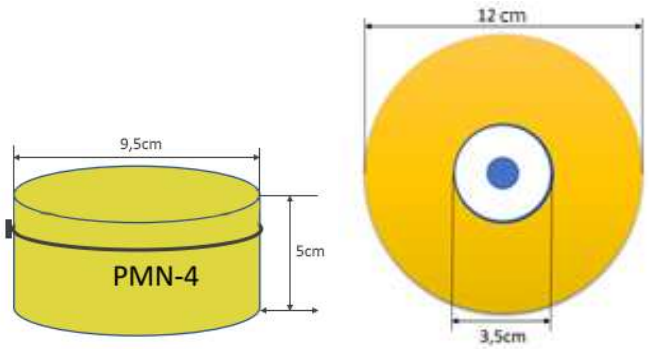

Figure 7: Dimensions of buried targets used for the experiments: (a) antipersonnel landmine PMN-4; (b) compact disk (CD) with a central hole (non-metallic) 3.5 cm in diameter.

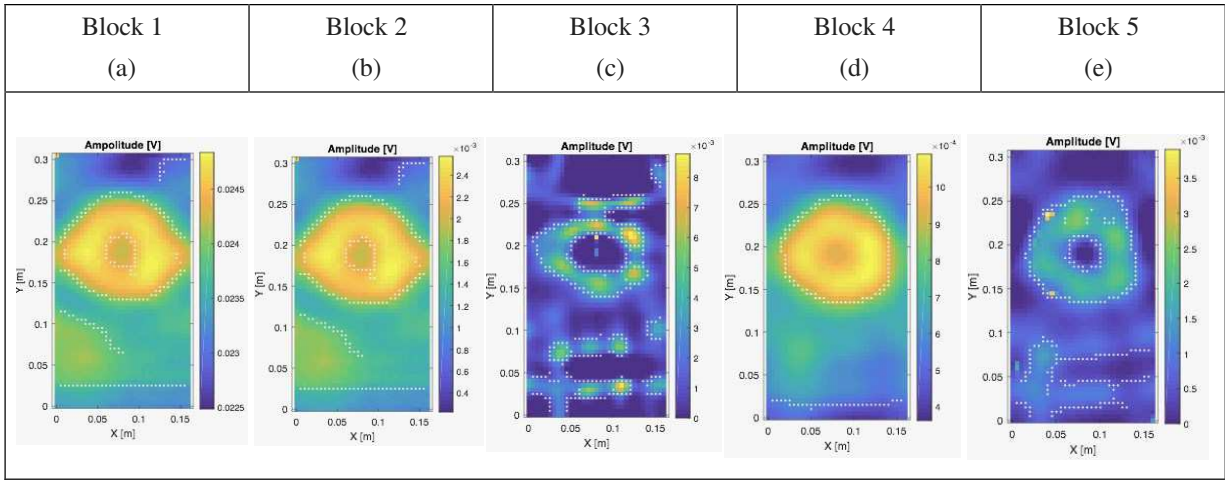

Figure 8: Voltage amplitude obtained by processing the CD scan data for each block of the algorithm shown in Figure 2. Focused image (d) at $z_0 = 3\,\text{cm}$.

in the interval from 0.3 mV to 2.5 mV, as expected.

In Figure 8(c), we can see the effects of the deconvolution with PSF_1 on the amplitude image. The dynamic range of image is improved (now at about 9 mV), and the shape of CD, in particular the central hole, is better highlighted.

In Figure 8(d) the result of the focusing algorithm at $z_0 = 3\,\text{cm}$ is shown. In the resulting image, the shape of the CD is less affected by lateral distortion.

Finally, the deconvolution of the radar print on the target plane (Figure 8(e)) enhances the contrast of the image and improves shape recognition of the object at the cost of small artefacts in two small regions on the edge of the CD. The origin of these artefacts is probably due to multiple reflection paths with the metal structure of the scanner and/or the sandbox.

Figure 9 shows the intensity profile along y direction at $x = 8\,\text{cm}$ (corresponding to the coordinate of the centre of CD) for the acquired hologram in blue, and the final image in red. The enhancement in the dynamic range in the focused image is clearly visible in this comparison. The width of signal at $-3\,\text{dB}$ from the peak is about 11 cm, compatible with the actual diameter of the CD.

The same sequence of amplitude images is shown in Figure 10, but for scanning of a PMN-4 mine simulant. This represents a typical actual target for which the algorithm has been conceived and developed. It should be noted that this target is not a planar reflector owing to its three-dimensional shape and the fact that its construction includes internal parts with differing electromagnetic characteristics — possibly making the focussed image less representative of the overall shape of the target, with particularly-reflective parts highlighted. Rather than a limitation, this could produce images that are characteristic signatures of different mines with differing internal

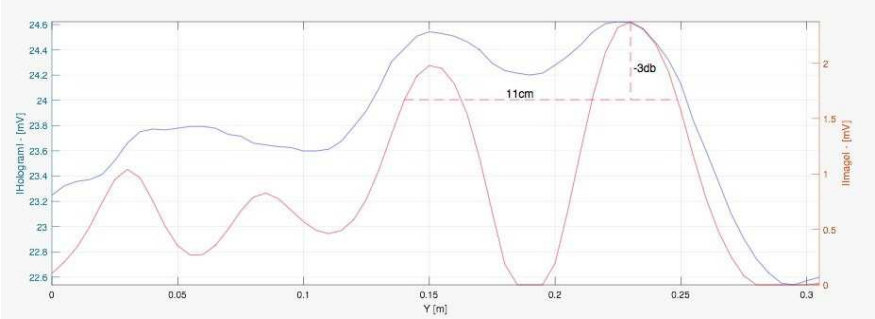

Figure 9: Intensity profile along y direction at $x = 8\,\text{cm}$ for the CD scan data.

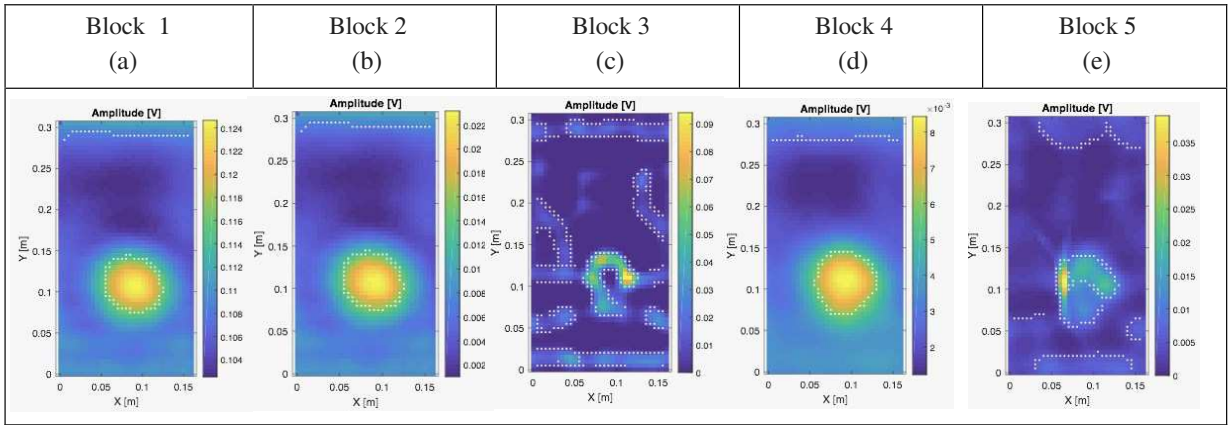

Figure 10: Voltage amplitude obtained by processing the PMN-4 scan data for each block of the algorithm shown in Figure 2. Focused image (d) is at $z_0 = 7\,\text{cm}$.

construction, and might eventually reduce false alarms from objects that have a mine-like shape, but no regular internal details. For example, round rocks of the same size as mines may be the most likely source of false alarms [9].

4. CONCLUSIONS

In this paper, we have described a signal processing scheme for a holographic radar antenna operating in a stand-off condition for landmine detection. We compare the results of our experimental measurements with the theoretical resolution of $\lambda/4$ which is typical for a ground-coupled scanning antenna. Additional information about the experimental conditions, such as the electromagnetic field distribution on the antenna aperture and radiation pattern, was used to enhance the image quality by reducing distortion due to defocussing and finite-size antenna effects. We carried out our experiments on a standard compact disk to characterize and understand the benefits obtained by the single blocks of the processing chain.

Our proposed imaging method is able to detect details significantly smaller than the radar wavelength and aperture size, as shown by the detection of the 3.5 cm diameter of the non-metallic area at the centre of the compact disk. The same processing method applied to a PMN-4 plastic landmine simulant at a distance of 7 cm revealed some advantages in image contrast and size estimation, even though this type of object is not a planar reflector, as assumed for the modelling the back-propagation of the electromagnetic field.

In order to identify easily unexploded ordnance using image interpretation, it is important to estimate both shape and dimensions of the buried objects. Images that reproduce internal construction details may be even more effective in reduce false alarm rates, and can assist with the subsequent steps in the demining operation following the detection and classification phase.

ACKNOWLEDGMENT

The authors wish to acknowledge the funding of the NATO project G5014 “Holographic and Impulse Subsurface Radar for Landmine and IED Detection”.

REFERENCES

1. Capineri, L., I. Arezzini, M. Calzolai, C. G. Windsor, I. Masaharu, T. D. Bechtel, and S. I. Ivashov, "High resolution imaging with a holographic radar mounted on a robotic scanner," *PIERS Proceedings*, 1583–1585, Stockholm, Sweden, Aug. 12–15, 2013.
2. Capineri, L., P. Falorni, T. Becthel, S. Ivashov, V. Razevig, and A. Zhuravlev, "Water detection in thermal insulating materials by high resolution imaging with holographic radar," *Measurement Science and Technology*, Vol. 28, No. 1, Jan. 2017.
3. Inagaki, M., T. D. Bechtel, S. I. Ivashov, and C. G. Windsor, "Analytical approach for RASCAN radar images of dinosaur footprints through basic experiments," *PIERS Proceedings*, 1586–1590, Stockholm, Sweden, Aug. 12–15, 2013.
4. Windsor, C., L. Capineri, and T. D. Bechtel, "Buried object classification using holographic radar," *Insight-Non-Destructive Testing and Condition Monitoring*, Vol. 54, No. 6, 331–339, 2012.
5. Boyer, A., P. Hirsch, J. Jordan, L. Lesem, and D. Rooy, "Reconstruction of ultrasonic images by backward propagation," *Acoustical Holography*, A. F. Metherell-Plenum Press, New York, 1971.
6. S. Xiaoji, S. Yi, Z. Yutao, H. Chunlin, and L. Min, "Improving holographic radar imaging resolution via deconvolution," *15th International Confrence on Ground Penetrating Radar — GPR 2014*, 2014.
7. Sheen, D., D. L. McMakin, and T. E. Hall, "Three-dimensional millimeter-wave imaging for concealed weapon detection," *IEEE Transactions on Microwave Theory and Techniques*, Vol. 49, No. 9, Sep. 2001.
8. Hu, M.-K., "Fresnel region fields of circula aperture antennas," *Journal of Research of the National Bureau of Standards — D. Radio Propagation*, Vol. 65D, No. 2, Mar., Apr. 1961.
9. Bechtel, T., L. Capineri, C. Windsor, M. Inagaki, and S. Ivashov, "Comparison of ROC curves for landmine detection by holographic radar with ROC data from other methods," *8th International Workshop on Advanced Ground Penetrating Radar (IWAGPR)*, Firenze, Italy, 2015.